[11] Kirk, D. R., Grayson, T., Garren, D., and Chong, C. Y. (2000)
AMSTE precision fire control tracking overview.
In *Proceedings of the IEEE Aerospace Conference*, Big Sky, MT, Mar. 2000.

[12] Kirubarajan, T., Bar-Shalom, Y., Blair, W. D., and Watson, G. A. (1998)
IMMPDA solution to benchmark for radar resource allocation and tracking in the presence of ECM.
IEEE Transactions on Aerospace and Electronic Systems, **34**, 3 (Oct. 1998), 1023–1036.

[13] Kirubarajan, T., Bar-Shalom, Y., Pattipati, K. R., and Kadar, I. (2000)
Ground target tracking with topography-based variable structure IMM estimator.
IEEE Transactions on Aerospace and Electronic Systems, **36**, 1 (Jan. 2000), 26–46.

[14] Li, X. R. (1996)
Hybrid estimation techniques.
In C. T. Leondes (Ed.), *Control and Dynamic Systems*, Vol. 76, San Diego, CA: Academic Press, 1996.

[15] Li, X. R., and Bar-Shalom, Y. (1996)
Multiple-model estimation with variable structure.
IEEE Transactions on Automatic Control, **41** (Apr. 1996), 478–493.

[16] Lin, H., and Atherton, D. P. (1993)
An investigation of the SFIMM algorithm for tracking maneuvering targets.
In *Proceedings of the 32nd IEEE Conference on Decision and Control*, San Antonio, TX, Dec. 1993, 930–935.

[17] Lin, L., Kirubarajan, T., and Bar-Shalom, Y. (2002)
New assignment-based data association for tracking move-stop-move targets.
In *Proceedings of the 5th International Conference on Information Fusion*, Annapolis, MD, July 2002.

[18] Maybeck, P. S., and Hentz, K. P. (1987)
Investigation of moving-bank multiple model adaptive algorithms.
AIAA Journal of Guidance, Control and Dynamics, **10** (Jan. 1987), 90–96.

[19] Mazor, E., Averbuch, A., Bar-Shalom, Y., and Dayan, J. (1998)
Interacting multiple model methods in target tracking: A survey.
IEEE Transactions on Aerospace and Electronic Systems, **34** (Jan. 1998), 103–123.

[20] Shea, P. J., Zadra, T., Klamer, D., Frangione, E., and Brouillard, R. (2000)
Precision tracking of ground targets.
In *Proceedings of the IEEE Aerospace Conference*, Big Sky, MT, Mar. 2000.

[21] Wang, H., Kirubarajan, T., and Bar-Shalom, Y. (1999)
Large scale air traffic surveillance using IMM estimators with assignment.
IEEE Transactions on Aerospace and Electronic Systems, **35**, 1 (Jan. 1999), 255–266.

[22] Yeddanapudi, M., Bar-Shalom, Y., and Pattipati, K. R. (1997)
IMM estimation for multitarget-multisensor air traffic surveillance.
IEEE Proceedings, **85**, 1 (Jan. 1997), 80–94.

Two-Parameter Bifurcation Analysis of Longitudinal Flight Dynamics

The bifurcation analysis of longitudinal flight dynamics is presented, emphasizing the influence of elevator deflection and aircraft mass. Based on a mathematical model proposed by Garrard and Jordan (1977), a rich variety of bifurcation phenomena such as saddle-node bifurcation, Hopf bifurcation, and cycle fold bifurcations are observed in the numerical simulations of longitudinal flight dynamics of the F-8 aircraft. The occurrence of saddle-node bifurcation and Hopf bifurcation may result in jump behavior and pitch oscillations of flight dynamics. The analysis leads to a division of the longitudinal flight space into several maneuvering regions, and may provide more understanding of the longitudinal flight dynamics.

I. INTRODUCTION

Recently, the nonlinear phenomena of flight dynamics has attracted considerable attention [1–8]. One of the main goals of the studies is to find a linkage between nonlinear aircraft motions, such as stall and divergent behaviors, and the possible bifurcation phenomena of the governing dynamic equations. For instance, both stationary and Hopf bifurcations are reported and studied in several aircraft models [1–6]. The stabilization of the trim condition of an aircraft arbitrarily close to the stall angle of the F-8 Crusader was studied, in a manner which also provides an impending stall warning signal to the pilot [7–8]. Such a signal is a small-amplitude and stable limit-cycle type pitching motion of the aircraft, which persists to within a prescribed margin of the impending divergent stall. It is known that the analysis of bifurcation phenomena is useful in understanding nonlinear system behavior. Through bifurcation analysis, the nonlinear behavior of aircraft at high angle-of-attack flight such as jump to new steady states, oscillations, and hysteresis, may be predicted. In [9], bifurcation theory was employed to analyze the nonlinear phenomena of longitudinal flight dynamics by choosing the elevator deflection and mass of the aircraft as system bifurcation parameters.

Manuscript received December 25, 2001; revised May 7, 2003; released for publication May 7, 2003.

IEEE Log No. T-AES/39/3/818516.

Refereeing of this contribution was handled by T. F. Roome.

This research was supported by the National Science Council, Taiwan, ROC under Grants NSC 84-2212-E009-002, NSC 89-CS-D-009-013 and NSC 91-2212-E-216-019.

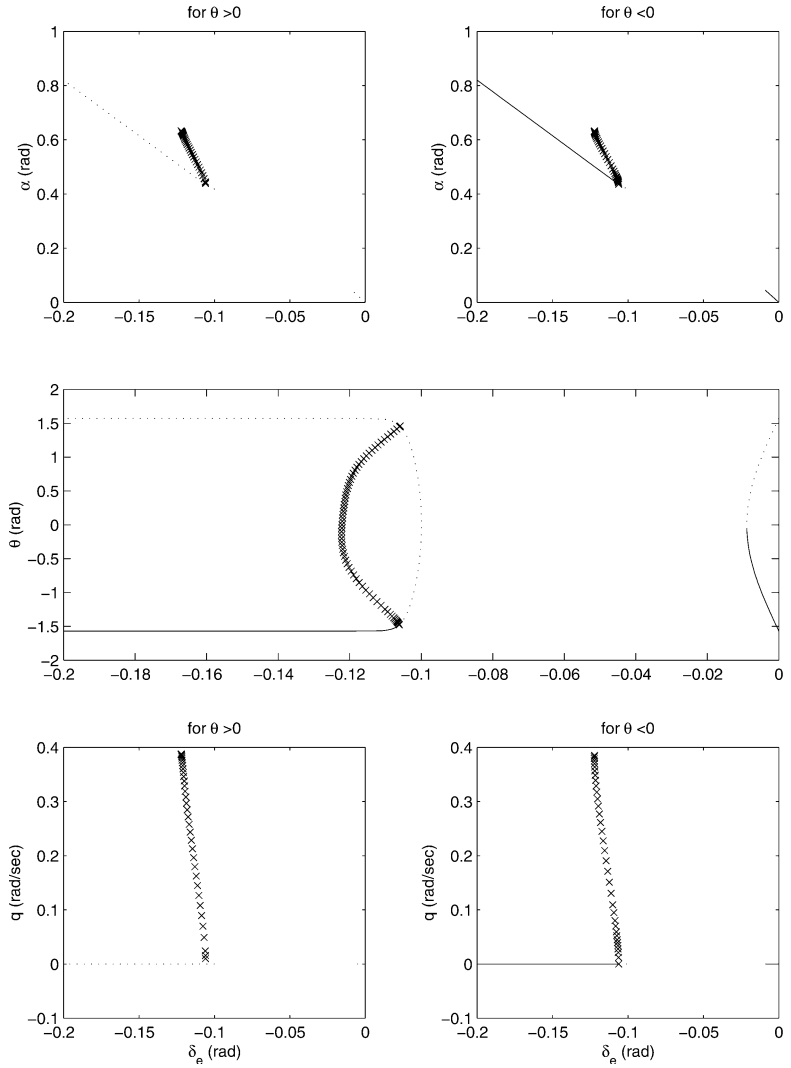

Fig. 1. System equilibria and periodic solutions for nominal third-order model.

In [9], the longitudinal flight dynamics were studied for a fixed setting of the mass of the aircraft. The analysis reveals that the saddle-node bifurcation and the Hopf bifurcation may result in jump behavior and pitch oscillation, respectively. This work continues the study of longitudinal flight dynamics developed by [9], emphasizing the combined effect of two control parameters: elevator deflection and mass of the aircraft. One of the main goals of this work is to identify and describe the relationship between the nonlinear behaviors of aircraft dynamics and the bifurcation phenomena arising from the governing dynamic equations. The analysis is carried out on the third-order model of the longitudinal dynamics for F-8 proposed in [10]. The analysis reveals that the longitudinal flight space might be separated into several maneuvering regions. Each of these regions possesses completely different nonlinear characteristics. Numerical continuation and bifurcation analysis package AUTO [11] and extensive computer simulations are employed to evaluate system behavior. The numerical techniques consist of the continuation of fixed points and limit cycles with respect to the mass of the aircraft, and the continuation of bifurcation-point branches of fixed points and limit cycles in the two-parameter plane. Phase diagrams are constructed by simulation to illustrate the distinctly different dynamical behaviors associated with each regime of the parameter space.

The paper is organized as follows. In Section II, we develop the model of the longitudinal flight dynamics. This is followed in Section III by the study of the flight dynamics for various settings of system parameters. In Section IV, the analysis of the two-parameter bifurcation is studied. Finally, concluding remarks are given in Section V.

II. MATHEMATICAL MODELS

In the following, we present the mathematical model for longitudinal flight dynamics from [10], which is employed in the analysis in the next two

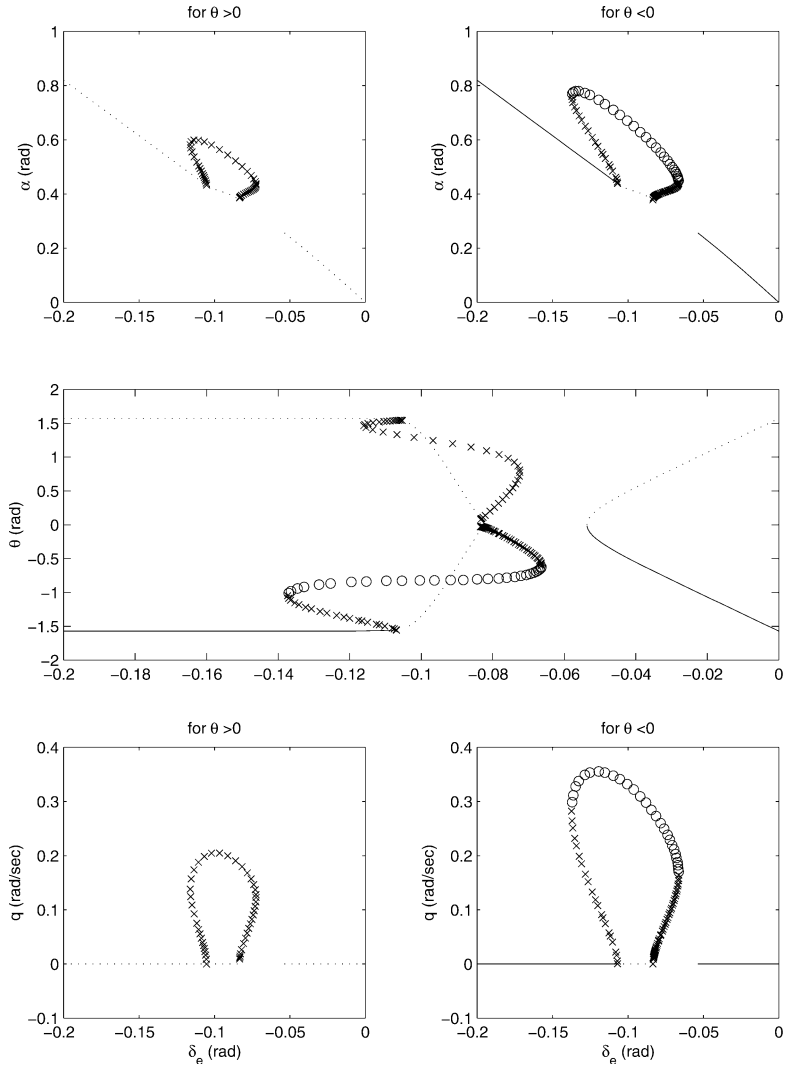

Fig. 2. System equilibra and periodic solutions for modified model with $m = 4.47m_0$.

sections. The drag is considered to be small compared with the lift and weight and is neglected in the analysis. The lift force is separated into its wing and tail components.

Based on these assumptions, the motion equations for longitudinal dynamics with thrust neglected are given by

$$m(\dot{u} + w\dot{\theta}) = -mg\sin\theta + L_w\sin\alpha + L_t\sin\alpha_t \quad (1a)$$

$$m(\dot{w} - u\dot{\theta}) = mg\cos\theta - L_w\cos\alpha - L_t\cos\alpha_t \quad (1b)$$

$$I_y\ddot{\theta} = M_w + lL_w\cos\alpha - l_tL_t\cos\alpha_t - c\dot{\theta} \quad (1c)$$

where

u	axial velocity
w	vertical velocity
α	wing angle of attack
α_t	tail angle of attack
θ	pitch angle
I_y	moment of inertia about axis
L_w	wing lift force
L_t	tail lift force
M_w	wing pitching moment
m	aircraft mass
l	distance between wing aerodynamic center and aircraft center of gravity
l_t	distance between tail wing aerodynamic center and aircraft center of gravity
$c\dot{\theta}$	damping moment.

It is known that the tail and wing lift forces can be given by

$$L_w = C_{L_w}QS \qquad \text{and} \qquad L_t = C_{L_t}QS_t,$$

where

C_{L_w}	coefficient of wing lift
C_{L_t}	coefficient of tail lift
Q	dynamic pressure
S	wing area
S_t	horizontal tail area.

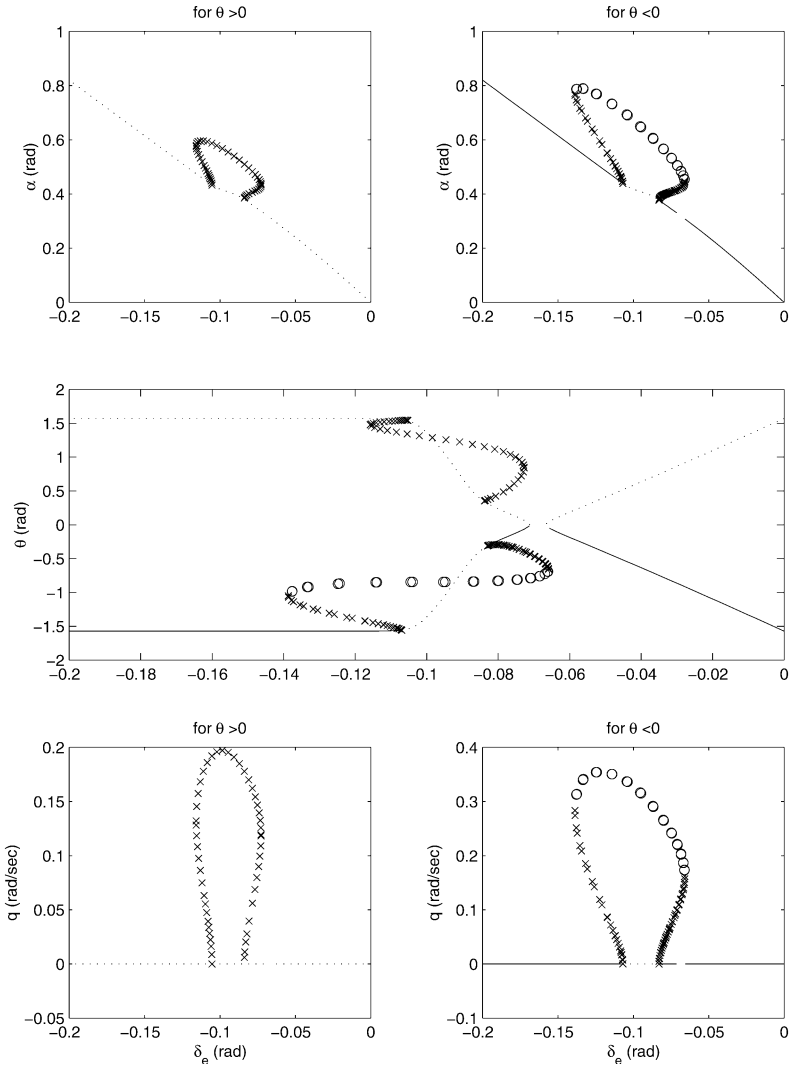

Fig. 3. System equilibra and periodic solutions for modified model with $m = 4.72m_0$.

Using

$$w = u\tan\alpha \qquad \text{and} \qquad \dot{w} = \dot{u}\tan\alpha + u\dot{\alpha}\sec^2\alpha \quad (2)$$

we can rewrite (1) as

$$\dot{u} = -u\dot{\theta}\tan\alpha - g\sin\theta + \frac{L_w}{m}\sin\alpha + \frac{L_t}{m}\sin\alpha_t \quad (3a)$$

$$\dot{\alpha} = \dot{\theta}\sin^2\alpha + \frac{g}{u}\sin\theta\sin\alpha\cos\alpha - \frac{L_w}{um}\sin^2\alpha\cos\alpha - \frac{L_t}{um}\sin\alpha\cos\alpha\sin\alpha_t + \dot{\theta}\cos^2\alpha + \frac{g}{u}\cos^2\alpha\cos\theta - \frac{L_w}{um}\cos^3\alpha - \frac{L_t}{um}\cos^2\alpha\cos\alpha_t \quad (3b)$$

$$\ddot{\theta} = \frac{M_w}{I_y} + \frac{lL_w}{I_y}\cos\alpha - \frac{l_tL_t}{I_y}\cos\alpha_t - \frac{c}{I_y}\dot{\theta}. \quad (3c)$$

Equation (3) represents the so-called "full (fourth-order) model" of longitudinal flight dynamics with states $(u, \alpha, \theta, \dot{\theta})$.

Given that the aircraft flies at a constant velocity and let $q := \dot{\theta}$, (3) can be reduced to a third-order model given by

$$\dot{\alpha} = q\cos^2\alpha + \frac{g}{u}\cos^2\alpha\cos\theta - \frac{L_w}{um}\cos^3\alpha - \frac{L_t}{um}\cos^2\alpha\cos\alpha_t \quad (4a)$$

$$\dot{\theta} = q \quad (4b)$$

$$\dot{q} = \frac{M_w}{I_y} + \frac{lL_w}{I_y}\cos\alpha - \frac{l_tL_t}{I_y}\cos\alpha_t - \frac{c}{I_y}q. \quad (4c)$$

Theoretical analysis of local dynamic behavior of the system (4) has been obtained in [9] by using system linearization and bifurcation theory. We focus here on the study of nonlinear phenomena for system (4) via numerical approach. Details are given in the next two sections.

III. LOCAL BIFURCATION ANALYSIS

In this section, we adopt the third-order model of [10] for F-8 aircraft. Based on this third-order model,

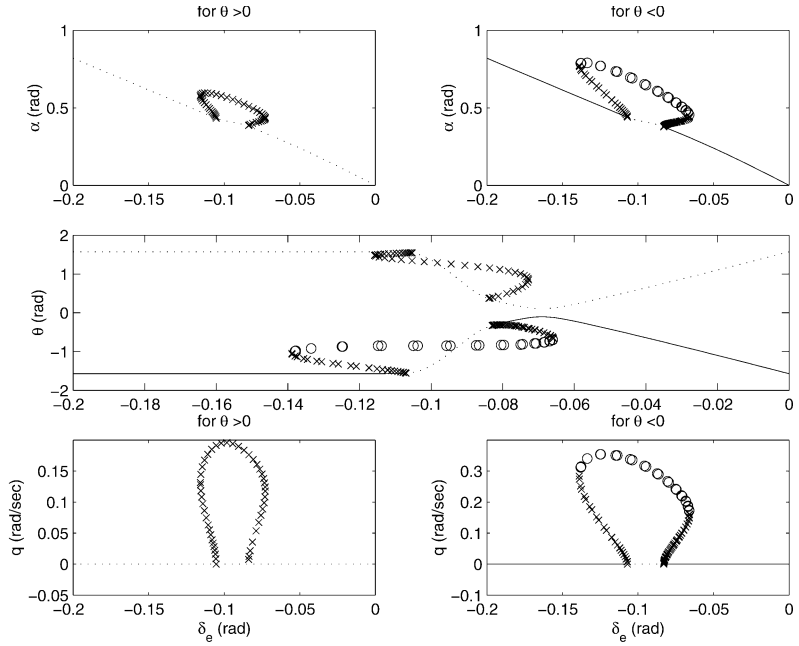

Fig. 4. System equilibria and periodic solutions for modified model with $m = 4.75m_0$.

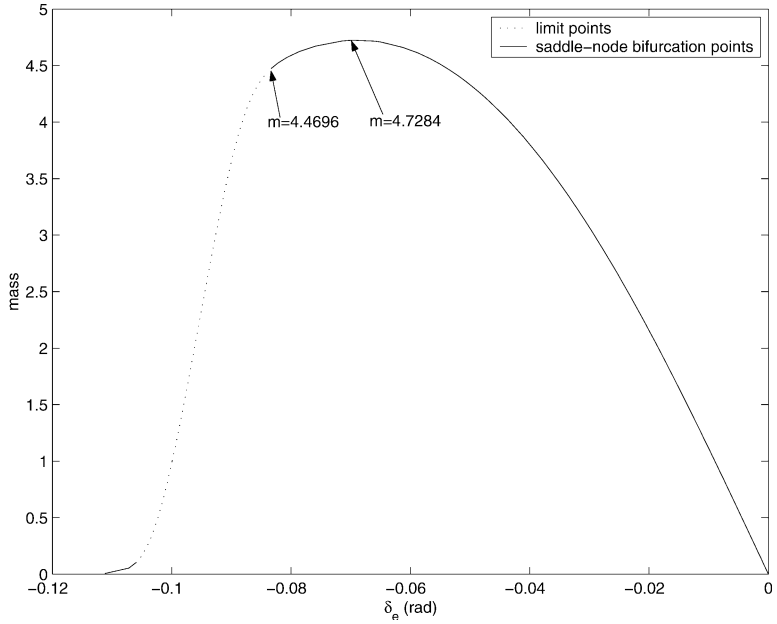

Fig. 5. Location of limit points in (m, δ_e) space.

the local stability and bifurcations of flight dynamics with respect to the variation of the tail deflection angle are obtained by numerical simulations. Details are given as below.

In [10], Garrard and Jordan proposed to approximate the wing lift and tail lift coefficients by two cubic polynomial functions, respectively, as given by

$$L_w = QS(C^1_{L_w}\alpha - C^2_{L_w}\alpha^3) \tag{5}$$

$$L_t = QS_t(C^1_{L_w}\alpha_t - C^2_{L_t}\alpha_t^3 + a_e\delta_e) \tag{6}$$

where δ_e represents the horizontal tail deflection angle measured clockwise from the x-axis and a_e is the linear approximation of the effect of δ_e on C_{L_t}. Since the horizontal tail of the F-8 is within the wing wake, the downwash angle ϵ has to be included in determining the tail angle-of-attack. Here, we adopt a linear approximation, $\epsilon = a_\epsilon\alpha$ from [10]. The tail angle-of-attack can then be given by

$$\alpha_t = \alpha - \epsilon + \delta_e = (1 - a_\epsilon)\alpha + \delta_e. \tag{7}$$

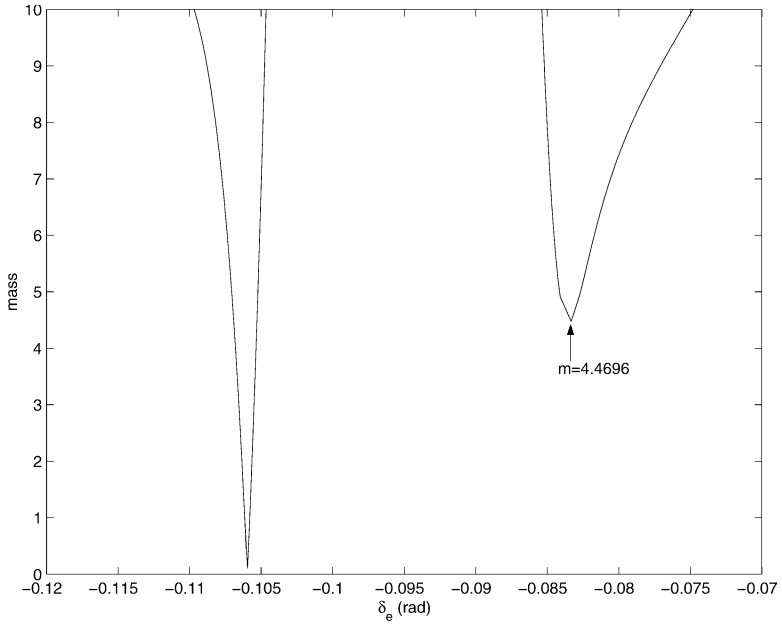

Fig. 6. Location of Hopf bifurcation points in (m,δ_e) space.

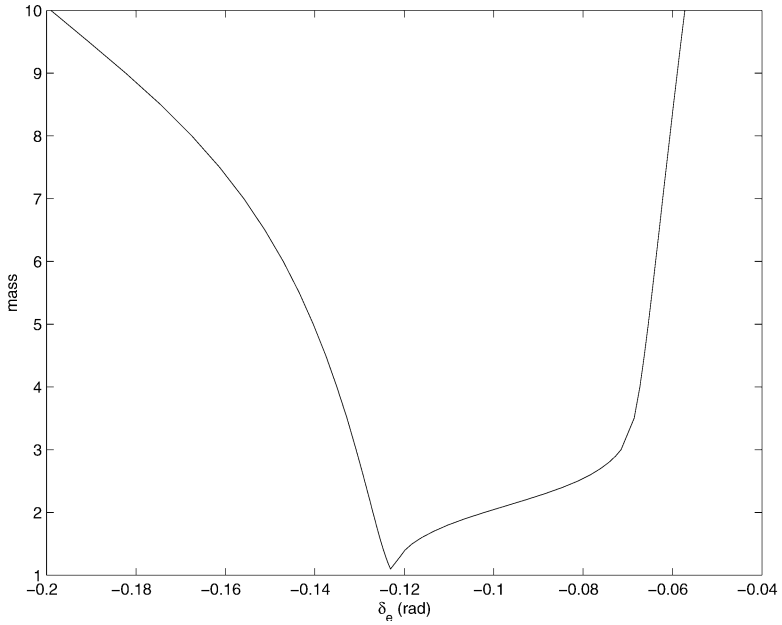

Fig. 7. Location of cyclic fold bifurcation points in (m,δ_e) space.

The aircraft data adopted from [10] is used in the following numerical study. Here, we assume the aircraft flies at constant velocity of u = 845.6 ft/s on altitude of 30,000 ft.

In [7–9], an approximation of the wing lift force coefficient is chosen to be closer to the realistic one in the stall and post-stall regions as given by

$$L_w = QS(C^1_{L_w}\alpha - C^2_{L_w}\alpha^3)\left[\frac{1}{1+\left(\frac{\alpha}{0.41}\right)^{60}}\right]. \quad (8)$$

For simplicity and without loss of generality, we assume the moment of inertia (I_y) is proportional to m. Adopting the wing lift coefficient as in (8), we can rewrite the system (4) as

$$\begin{aligned}\dot{\alpha} &= q\cos^2\alpha + 0.0381\cos^2\alpha\cos\theta \\ &\quad - \frac{1}{m}(564.434\alpha - 1693.301\alpha^3)\cdot\cos^3\alpha\cdot W \\ &\quad - \frac{1}{m}(35.145\alpha - 6.560\alpha^3 + 144.096\delta_e \\ &\qquad - 79.077\alpha^2\delta_e - 316.309\alpha\delta_e^2 - 421.745\delta_e^3) \\ &\quad \times\cos^2\alpha\cos(0.25\alpha + \delta_e) \quad (9a)\end{aligned}$$

$$\dot{\theta} = q \quad (9b)$$

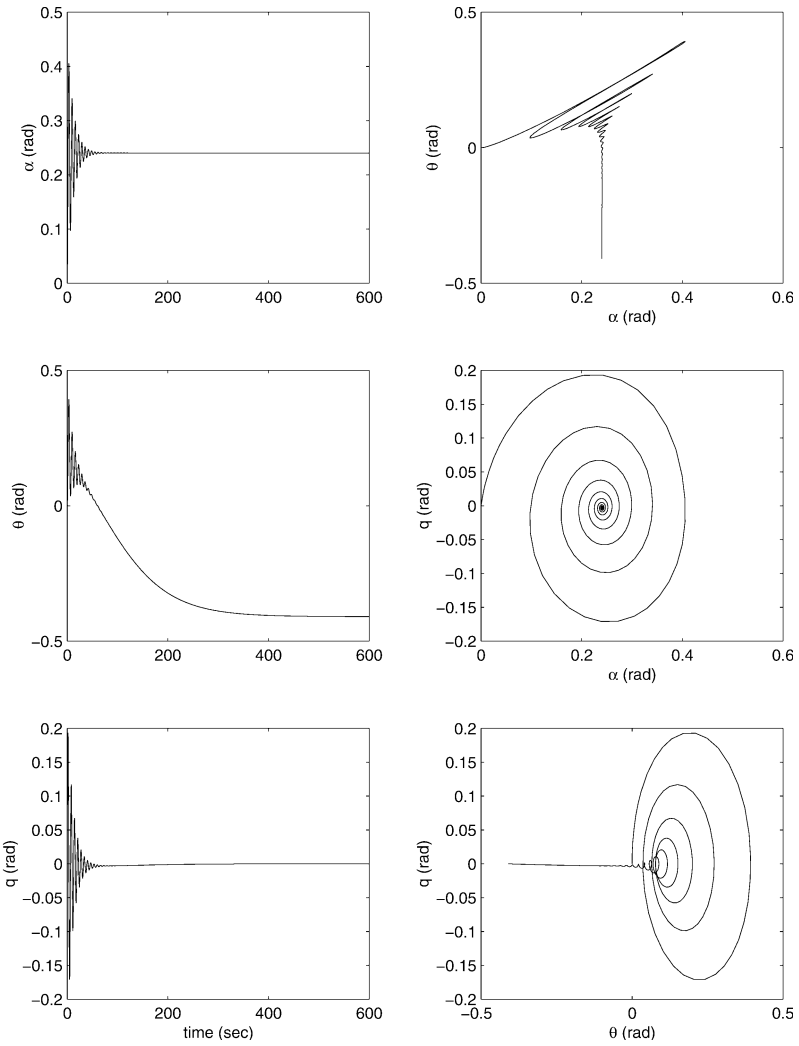

Fig. 8. System responses in time history and phase plane for $m = 4.72m_0$ at $\delta_e = -0.05$.

$$\dot{q} = -\frac{1}{m}264.409q + \frac{1}{m}(622.222\alpha - 1866.667\alpha^3)\cdot\cos\alpha\cdot W - \frac{1}{m}(3423.386\alpha - 641.885\alpha^3 + 14035.883\delta_e - 7702.619\alpha^2\delta_e - 30810.476\alpha\delta_e^2 - 41080.634\delta_e^3) \times \cos(0.25\alpha + \delta_e), \quad (9c)$$

where

$$W := \left[\frac{1}{1 + \left(\frac{\alpha}{0.41}\right)^{60}}\right].$$

First, we analyze the stability and local bifurcations of the system (9) by treating δ_e as principal system parameter and fixing another parameter m at different setting values. By using code AUTO, we find that the various bifurcations occurred in the system (9) with respect to the system parameters change. The locations of these bifurcations are also varied. In the following numerical study, the figures show the equilibrium points and periodic solutions that emerge from the bifurcation point of the system (9) for distinct parameter condition in the system parameter $\delta_e \in [-0.2, 0]$, where

"_____" (solid line)	stable equilibrium point,
"– – –" (dotted line)	unstable equilibrium point,
"o" (circle)	stable limit cycle,
"x" (cross)	unstable limit cycle.

Denote m_0 the original mass of the F-8 aircraft. Fig. 1 shows the bifurcation diagram for the condition of $m = m_0$. As observed in Fig. 1, there are two limit points and two Hopf bifurcation points of which one is stable and the other is unstable. The equilibrium points are found to disappear between two limit points, while the limit point on the right-hand side is a saddle-node bifurcation point.

The bifurcation diagram for the condition of $m = 4.47m_0$ is depicted in Fig. 2. Two pairs of Hopf bifurcation points are observed and the limit cycle folded up in one side become stable. As the value of the mass m increases, the left limit point becomes a saddle-node bifurcation point at the parameter value $m > 4.5m_0$ as presented in Fig. 3.

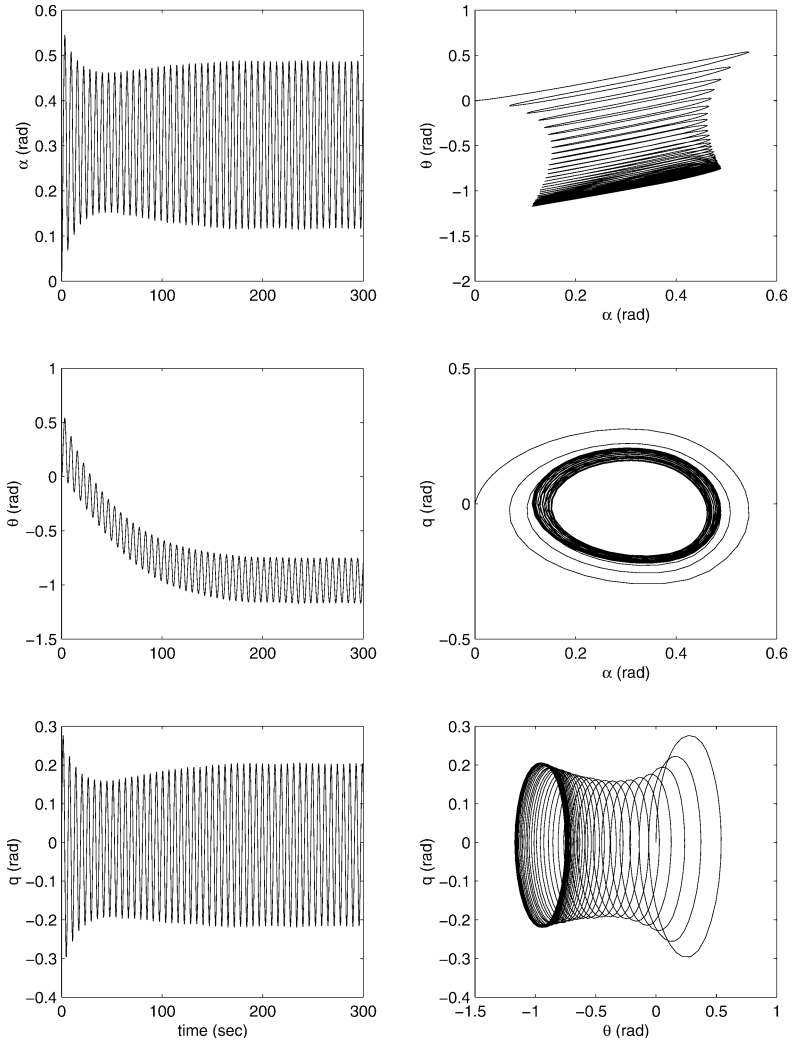

Fig. 9. System responses in time history and phase plane for $m = 4.72m_0$ at $\delta_e = -0.069$.

It is interesting to note that the stable limit cycle crosses the discontinuity of equilibrium points at the parameter value of $m = 4.72m_0$ as depicted in Fig. 3. This might provide a solution of connecting the jump behavior between two saddle-node bifurcation points as δ_e varies. Fig. 4 presents that the discontinuity of system equilibria disappears at the parameter value of $m = 4.75m_0$. Here, two saddle-node bifurcation points are disappeared while the two pairs of Hopf bifurcation still exist.

From the above numerical study, it is concluded that the parameter m may play an important role in longitudinal flight dynamics. In the next section, two-parameter bifurcation analysis of system (9) is carried out by treating both of the elevator deflection δ_e and the mass m as system parameters.

IV. TWO-PARAMETER BIFURCATION ANALYSIS

As presented in Section III, we know that aircraft mass m will affect the existence of equilibrium points. By doing rigorous simulations with different setting value of m, we find that the two limit points of system (9) close to each other as mass increases and vanishes at the new value of mass as $m \cong 4.7284m_0$ as depicted in Fig. 5. It is also observed from Fig. 5 that one of the two limit points is a saddle-node bifurcation point for $m \leq 4.4696m_0$, while both of the two limit points happen to be saddle-node bifurcation points for $4.4696m_0 \leq m \leq 4.7284m_0$. As observed in simulations, not only the limit points will move, but also the bifurcation points are rearranged as parameter values vary. Moreover, the system (9) produces two additional new bifurcation points for $\theta < 0$ and $\theta > 0$, respectively, for $m = 4.4696m_0$, and the periodic solutions emerging from these bifurcation points couple for each pair of Hopf bifurcations. Fig. 6 indicates the location of Hopf bifurcation points of m versus δ_e. It is found from Fig. 6 that two additional Hopf bifurcation points appear at $m > 4.4696m_0$ corresponding to $\theta > 0$ and $\theta < 0$. The location of cyclic fold bifurcation in two parameter space is also depicted in Fig. 7.

From Fig. 1, the angle of attack is found to be limited within about 0.01 rad and the aircraft

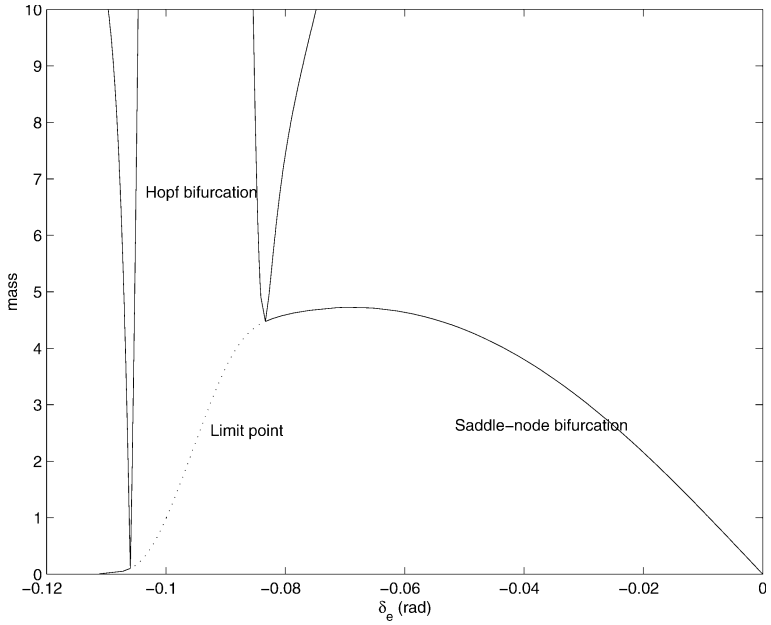

Fig. 10. Operation regime of longitudinal flight dynamics in (m,δ_e) space.

may lose its stability as the elevator deflection angle δ_e increases in order to attain larger angle-of-attack. Motivated by the simulation results, the angle-of-attack is found to be increased without loss of stability by varying the elevator deflection angle δ_e and aircraft mass m . For instance, as depicted in Fig. 3 for $m = 4.72m_0$, the location of the stable limit cycle and that of the equilibrium point overlap at $\delta_e = -0.066$. In such a case, the angle-of-attack can be promoted by changing the value of δ_e though there are no stable equilibrium points between the two saddle-node Hopf points for negative pitch angle θ. Indeed, as δ_e decreases from zero, the states will first remain at stable equilibrium point, and then jump to the stable limit cycle when δ_e crosses the first critical value at which a saddle-node bifurcation occurs. As δ_e decreases further, the oscillation will continue until δ_e crosses the second critical value at which the left saddle-node-Hopf bifurcation (or the so-called "cyclic-fold" bifurcation point) occurs. The system states will then converge to a stable equilibrium again, and the angle-of-attack can be increased efficiently by controlling the value of δ_e. A hysteresis phenomenon will occur if we reverse the changes of the elevator deflection angle. Figs. 8 and 9 show the typical time responses of the system states before and after δ_e crosses the first saddle-node bifurcation point. The system states converge to the stable equilibrium point for $\delta_e = -0.05$ as in Fig. 8, while they converge to a stable limit cycle for $\delta_e = -0.069$ as depicted in Fig. 9.

Fig. 10 depicts that the longitudinal flight dynamics can be divided into several maneuvering regions in the two-parameter space. This diagram will be useful in providing more understanding of the longitudinal flight dynamics. As the values of δ_e and m are chosen, the corresponding type and/or location of bifurcation phenomena can be determined by the diagram as in Fig. 10. The simulations presented in Sections III and IV demonstrate the distinct bifurcation phenomena as well as different dynamical behaviors within each regime of parameter space.

V. CONCLUSIONS

In this paper, we have investigated the bifurcation analysis of longitudinal flight dynamics with respect to two important control parameters: the elevator deflection δ_e and the mass of the aircraft m. Nonlinear phenomena, such as saddle-node bifurcation and Hopf bifurcation, are observed in the numerical simulation results for the dynamics of the F-8 aircraft as system parameters vary. The occurrence of saddle-node bifurcation and Hopf bifurcation may result in jump behavior and pitch oscillations. These results agree with previous observations presented in existing literatures [1–6]. The discontinuity of the system equilibrium caused by these bifurcations might contribute to the sudden jump behavior in pitch axis dynamics. Such observations might be very important for the design of fighter aircraft when the mass change becomes significant.

DER-CHERNG LIAW
Dept. of Electrical and Control Engineering
National Chiao Tung University
Hsinchu 300
Taiwan, ROC
E-mail: (dcliaw@cc.nctu.edu.tw)

CHAU-CHUNG SONG
Dept. of Electrical Engineering
Chung Hua University
Hsinchu 300
Taiwan, ROC

YEW-WEN LIANG
WEN-CHING CHUNG
Dept. of Electrical and Control Engineering
National Chiao Tung University
Hsinchu 300
Taiwan, ROC

REFERENCES

[1] Carroll, J. V., and Mehra, R. K. (1982)
Bifurcation analysis of nonlinear aircraft dynamics.
Journal of Guidance, Control, and Dynamics, **5**, 5 (1982), 529–536.

[2] Planeaux, J. B., and Barth, T. J. (1988)
High angle-of-attack dynamic behavior of a model high performance fighter aircraft.
AIAA Paper 88-4368, Aug. 1988.

[3] Planeaux, J. B., Beck, J. A., and Baumann, D. D. (1990)
Bifurcation analysis of a model fighter aircraft with control augmentation.
AIAA Paper 90-2836, Aug. 1990.

[4] Avanzini, G., and de Matteis, G. (1997)
Bifurcation analysis of a highly augmented aircraft model.
Journal of Guidance, Control, and Dynamics, **20**, 4 (1997), 754–759.

[5] Gibson, L. P., Nichols, N. K., and Litteboy, D. M. (1998)
Bifurcation analysis of eigenstructure assignment control in a simple nonlinear aircraft model.
Journal of Guidance, Control, and Dynamics, **21**, 5 (1998), 792–798.

[6] Jahnke, C. C., and Culick, F. E. C. (1994)
Application of bifurcation theory to the high angle-of-attack dynamics of the F-14.
Journal of Aircraft, **31**, 1 (1994), 26–34.

[7] Abed, E. H., and Lee, H-C. (1990)
Nonlinear stabilization of high angle-of-attack flight dynamics using bifurcation control.
In *Proceedings of the 1990 American Control Conference*, IEEE Publications, Piscataway, NJ, 1990, 2235–2238.

[8] Lee, H-C., and Abed, E. H. (1991)
'Washout filters in the bifurcation control of high alpha flight dynamics.
In *Proceedings of the 1991 American Control Conference*, IEEE Publications, Piscataway, NJ, 1991, 206–211.

[9] Liaw, D-C., and Song, C-C. (2001)
Analysis of longitudinal flight dynamics: A bifurcation-theoretic approach.
Journal of Guidance, Control, and Dynamics, **24**, 1 (2001), 109–116.

[10] Garrard, W. L., and Jordan, J. M. (1977)
Design of nonlinear automatic flight control systems.
Automatica, **13**, 5 (1977), 497–505.

[11] Doedel, E. J. (1986)
AUTO 86 User Manual.
Computer Science Dept., Concordia University, Jan. 1986.

ERRATA: Charge Equalization for Series-Connected Batteries[1]

Figures 5, 6, and 7 should be replaced with the figure below and the figures on the following page, as the distinction between active and inactive subcircuits in various modes was not as clear as desired.

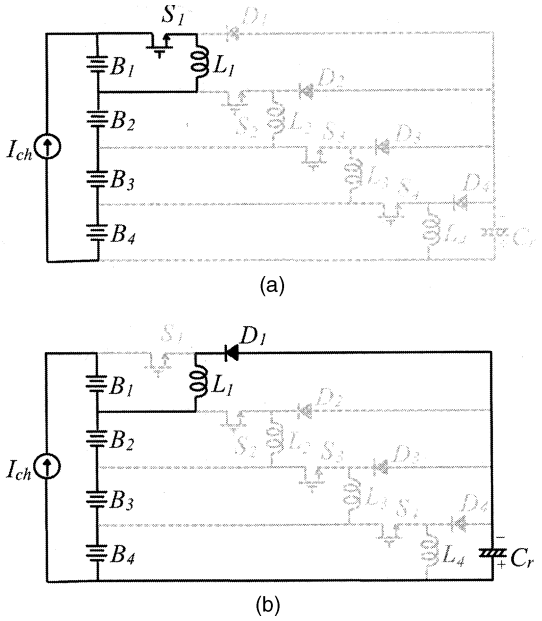

Fig. 5. Operation modes for activating subcircuits E_1. (a) Mode I. (b) Mode II.

[1]Moo, C. S., Hsieh, Y. C., and Tsai, I. S. (2003), *IEEE Transactions of Aerospace and Electronic Systems*, **39**, 2 (Apr. 2003), 704–710.

Manuscript received May 1, 2003.

IEEE Log No. T-AES/39/3/818517.

Authors' current addresses: C. S. Moo and Y. C. Hsieh, Power Electronics Laboratory, Dept. of Electrical Engineering, National Sun Yat-Sen University, Kaohsiung, Taiwan 804, ROC, E-mail: (mooxx@mail.ee.nsysu.edu.tw); I. S. Tsai, Dept. of Test and Measurement BU, Chroma ATE Inc., Taipei, Taiwan, ROC.